

**SUPPORTING INFORMATION**

**Structures and Bonding of Early Transition Metallaborane Clusters**

*Stuthee Mohapatra,<sup>†</sup> Sourav Gayen,<sup>†</sup> Ranjit Bag,<sup>†</sup> Arpita Das,<sup>†</sup> Rongala Ramalakshmi,<sup>†</sup> Marie Cordier,<sup>#</sup> and Sundargopal Ghosh<sup>\*,†</sup>*

*<sup>†</sup> Department of Chemistry, Indian Institute of Technology Madras, Chennai 600036, India. Tel: +91 44- 22574230; E-mail: [sghosh@iitm.ac.in](mailto:sghosh@iitm.ac.in)*

*<sup>#</sup> Univ Rennes, CNRS, Institut des Sciences Chimiques de Rennes, UMR 6226, F-35000 Rennes, France*

## Table of contents

### I.1 Supplementary Data

Scheme S1 Synthesis of compound **9**.

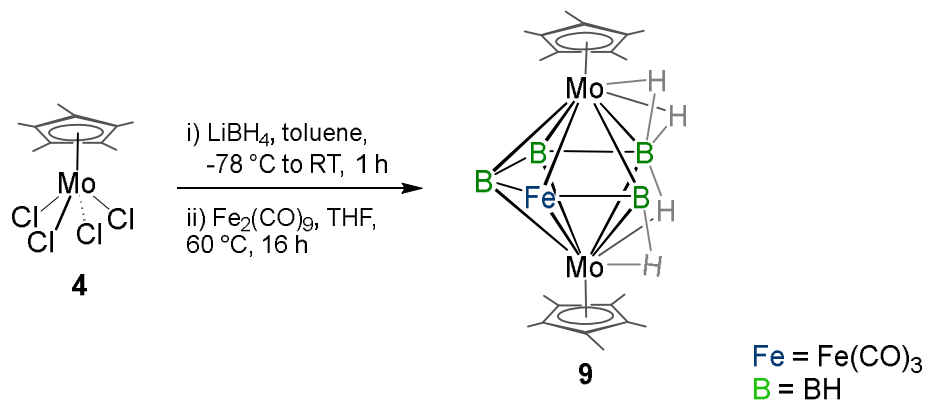
### I.2 Spectroscopic Details

- Figure S1  $^{11}\text{B}\{^1\text{H}\}$  NMR spectrum of compound **2**.
- Figure S2  $^1\text{H}$  NMR spectrum of compound **2**.
- Figure S3  $^1\text{H}/^{11}\text{B}\{^1\text{H}\}$  HSQC spectrum of compound **2**.
- Figure S4  $^{13}\text{C}\{^1\text{H}\}$  NMR spectrum of compound **2**.
- Figure S5 ESI-MS spectrum of compound **2** in  $\text{CH}_2\text{Cl}_2$  and MeOH mixture.
- Figure S6 IR spectrum of compound **2**.
- Figure S7  $^{11}\text{B}\{^1\text{H}\}$  NMR spectrum of compound **5**.
- Figure S8  $^1\text{H}$  NMR spectrum of compound **5**.
- Figure S9  $^{13}\text{C}\{^1\text{H}\}$  NMR spectrum of compound **5**.
- Figure S10 ESI-MS spectrum of compound **5** in  $\text{CH}_2\text{Cl}_2$  and MeOH mixture.
- Figure S11 IR spectrum of compound **5**.
- Figure S12  $^{11}\text{B}\{^1\text{H}\}$  NMR spectrum of compound **6**.
- Figure S13  $^1\text{H}$  NMR spectrum of compound **6**.
- Figure S14  $^{13}\text{C}\{^1\text{H}\}$  NMR spectrum of compound **6**.
- Figure S15 ESI-MS spectrum of compound **6** in  $\text{CH}_2\text{Cl}_2$  and MeOH mixture.
- Figure S16 IR spectrum of compound **6**.
- Figure S17  $^{11}\text{B}\{^1\text{H}\}$  NMR spectrum of compound **8**.
- Figure S18  $^1\text{H}$  NMR spectrum of compound **8**.
- Figure S19  $^{13}\text{C}\{^1\text{H}\}$  NMR spectrum of compound **8**.
- Figure S20 ESI-MS spectrum of compound **8** in  $\text{CH}_2\text{Cl}_2$  and MeOH mixture.
- Figure S21 IR spectrum of compound **8**.
- Figure S22  $^{11}\text{B}\{^1\text{H}\}$  NMR spectrum of compound **9**.
- Figure S23  $^1\text{H}$  NMR spectrum of compound **9**.
- Figure S24  $^{13}\text{C}\{^1\text{H}\}$  NMR spectrum of compound **9**.
- Figure S25 ESI-MS spectrum of compound **9** in  $\text{CH}_2\text{Cl}_2$  and MeOH mixture.
- Figure S26 IR spectrum of compound **9**.

## II Computational Data

- Table S1 Selected geometrical parameters and Wiberg bond indices (WBI) of **2**, **I**, **II**, **5** and **6**.
- Table S2 Comparison between experimental and theoretical chemical shifts of compounds **2**, **I**, **5** and **6**.
- Table S3 Calculated natural charges ( $q_M$ ,  $q_B$  and  $q_E$ ), natural valence population (Pop) and HOMO–LUMO gaps of **2**, **I**, **II**, **5**, and **6**.
- Figure S27 Comparison of HOMO-LUMO gap in **2**(a), **I**(b), **II**(c).
- Figure S28 Selected frontier molecular orbitals of **5**.
- Figure S29 Selected natural bonding orbitals of **5**.
- Figure S30 Selected frontier molecular orbitals of **6**.
- Figure S31 Optimized geometry of **2**.
- Figure S32 Optimized geometry of **I**.
- Figure S33 Optimized geometry of **II**.
- Figure S34 Optimized geometry of **5**.
- Figure S35 Optimized geometry of **6**.

## I.1 Supplementary Data



**Scheme S1** Synthesis of compound **9**.

## I.2 Spectroscopic details

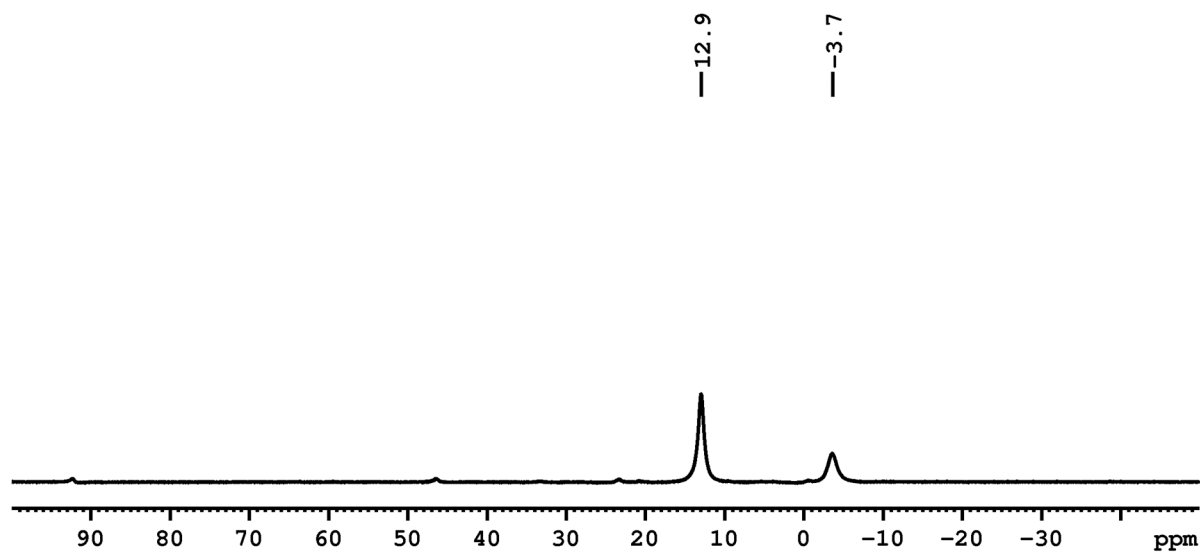


**Figure S1.**  $^{11}\text{B}\{^1\text{H}\}$  NMR spectrum of compound 2.

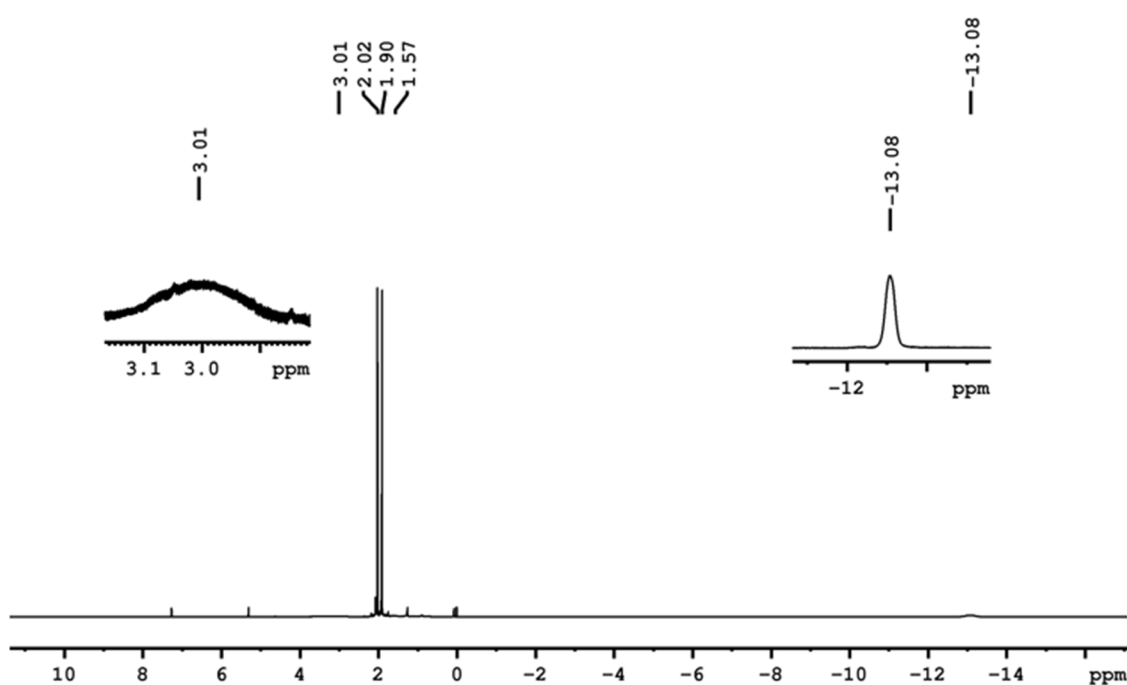


**Figure S2.**  $^1\text{H}$  NMR spectrum of compound 2.

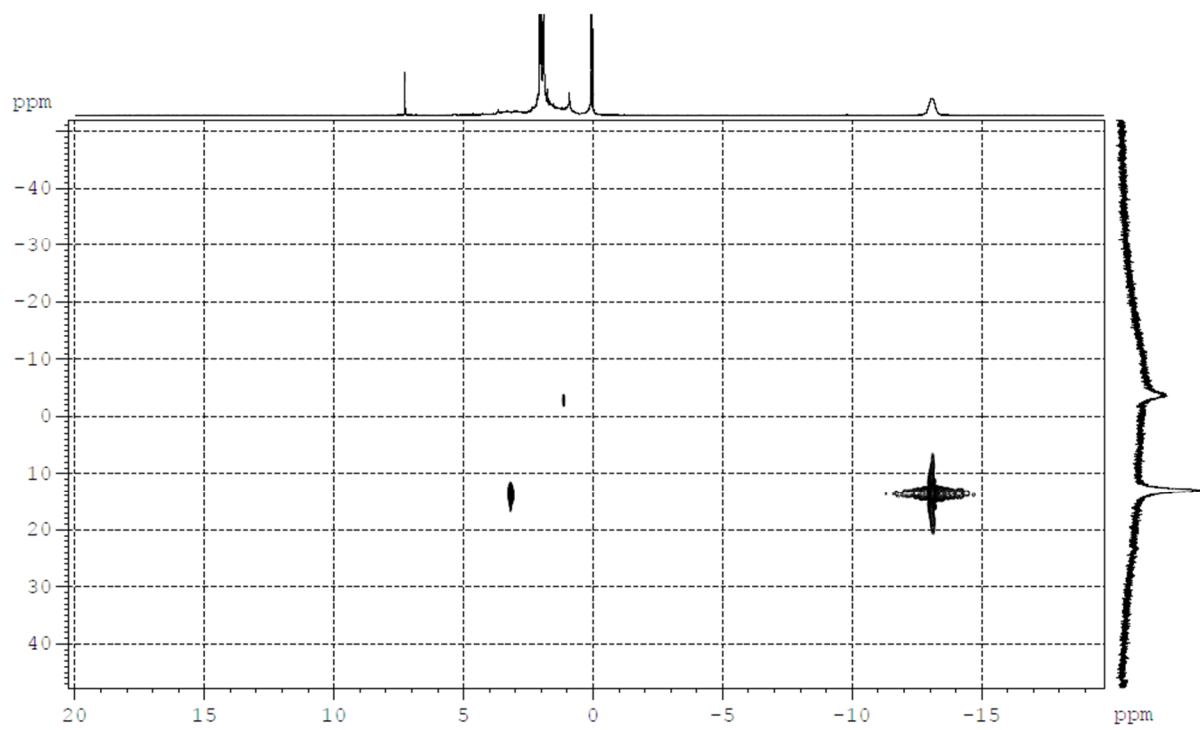


**Figure S3.**  $^1\text{H}/^{11}\text{B}\{^1\text{H}\}$  HSQC spectrum of compound 2.

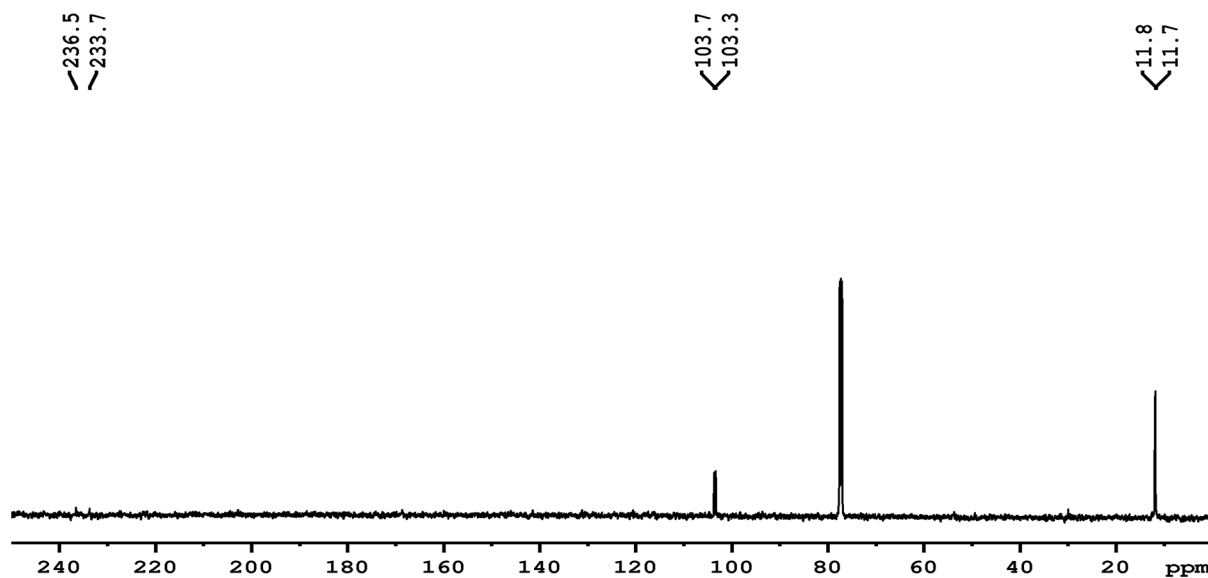


**Figure S4.**  $^{13}\text{C}\{^1\text{H}\}$  NMR spectrum of compound 2.

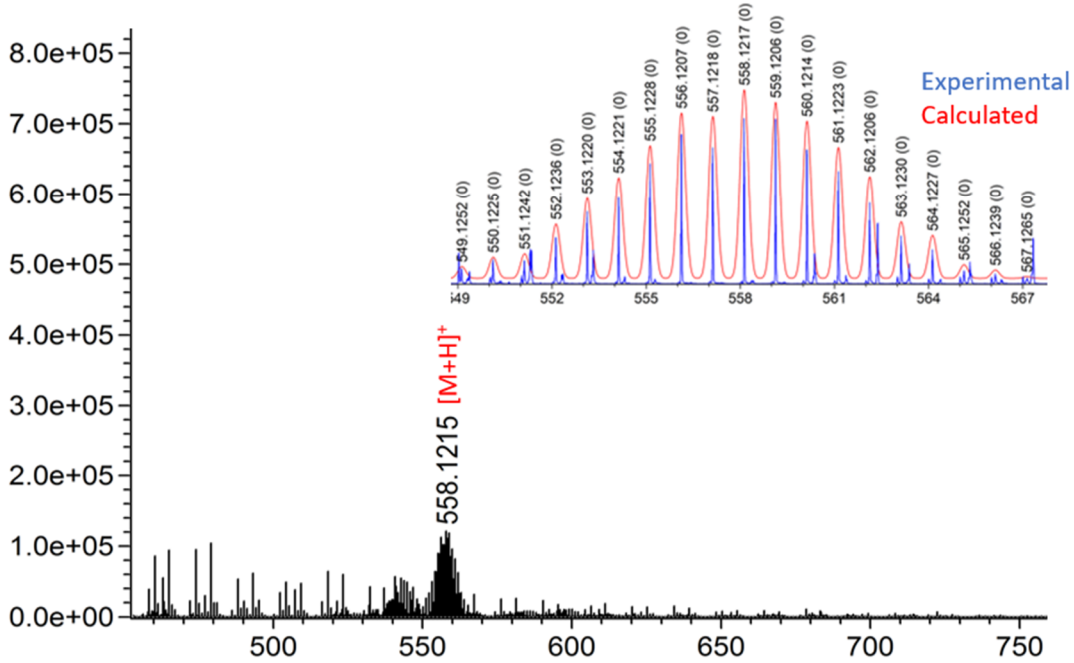


**Figure S5.** ESI-MS spectrum of compound **2** in CH<sub>2</sub>Cl<sub>2</sub> and MeOH mixture.

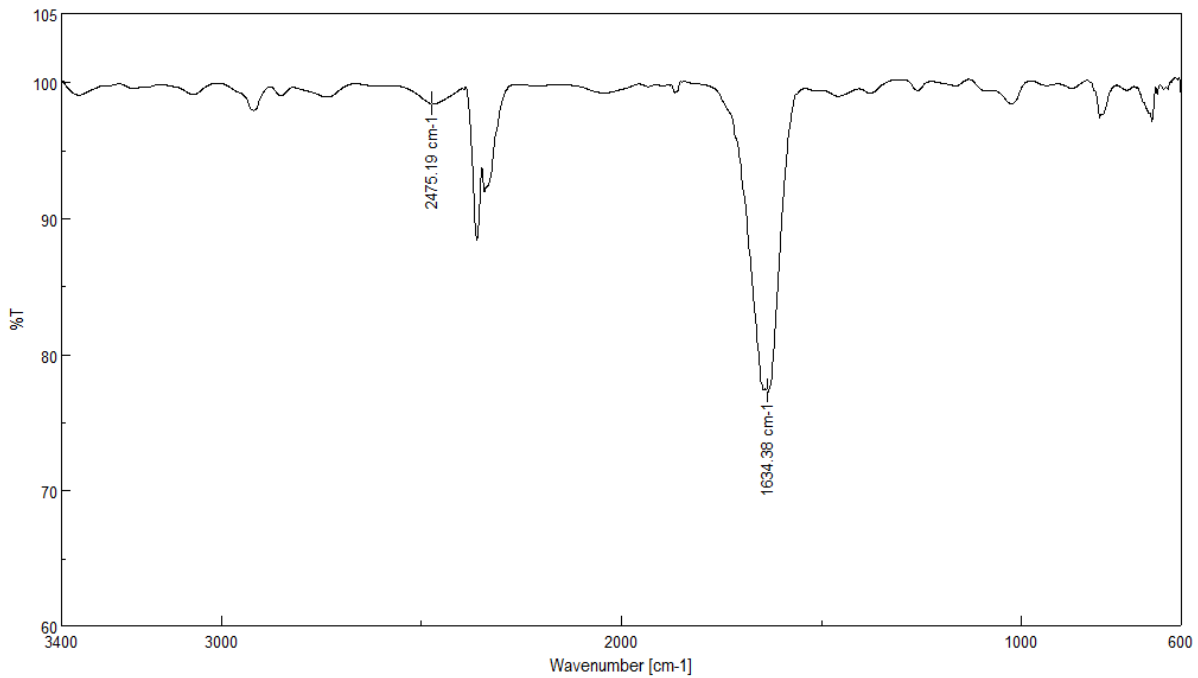


**Figure S6.** IR spectrum of compound **2**

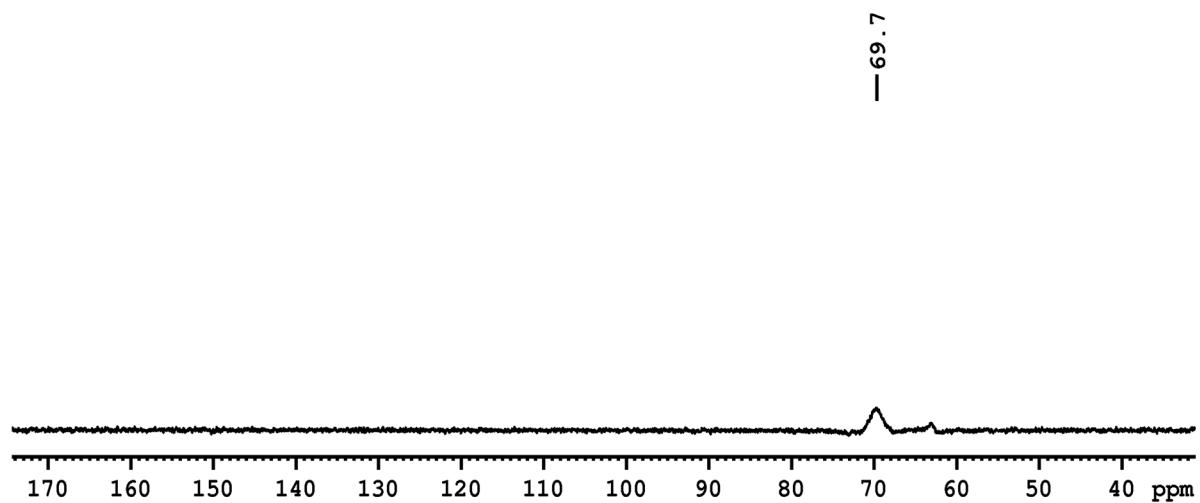


**Figure S7.**  $^{11}\text{B}\{^1\text{H}\}$  NMR spectrum of compound 5.

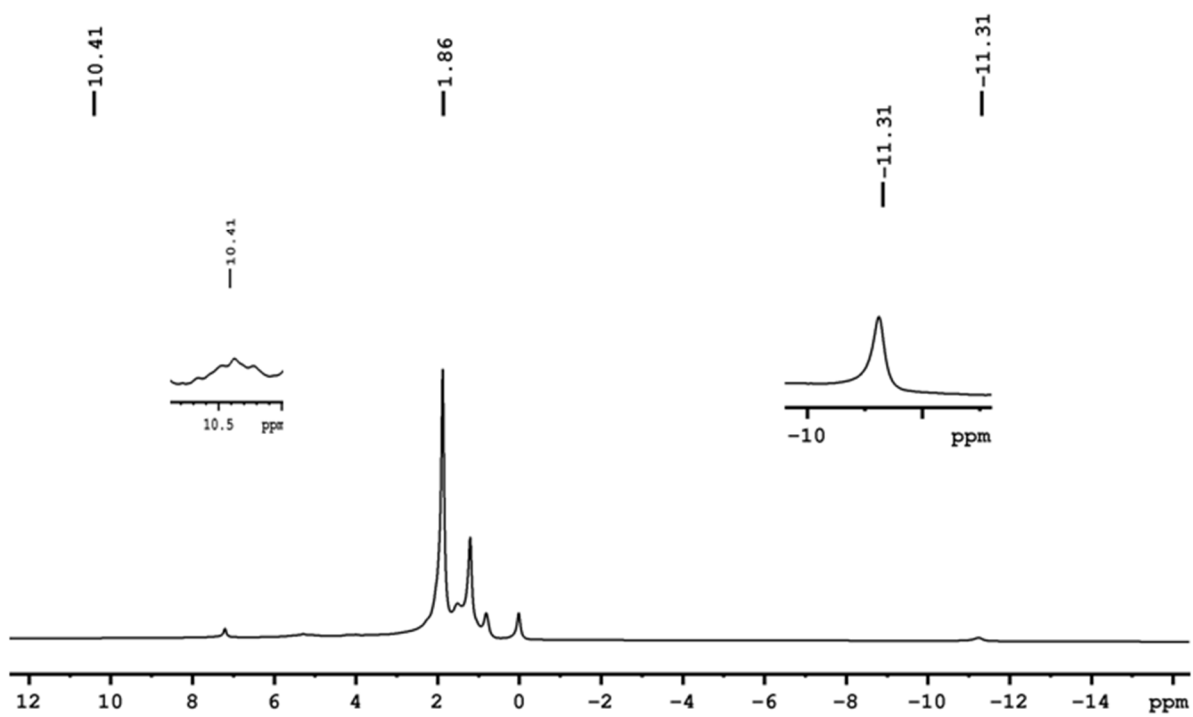


**Figure S8.**  $^1\text{H}$  NMR spectrum of compound 5.

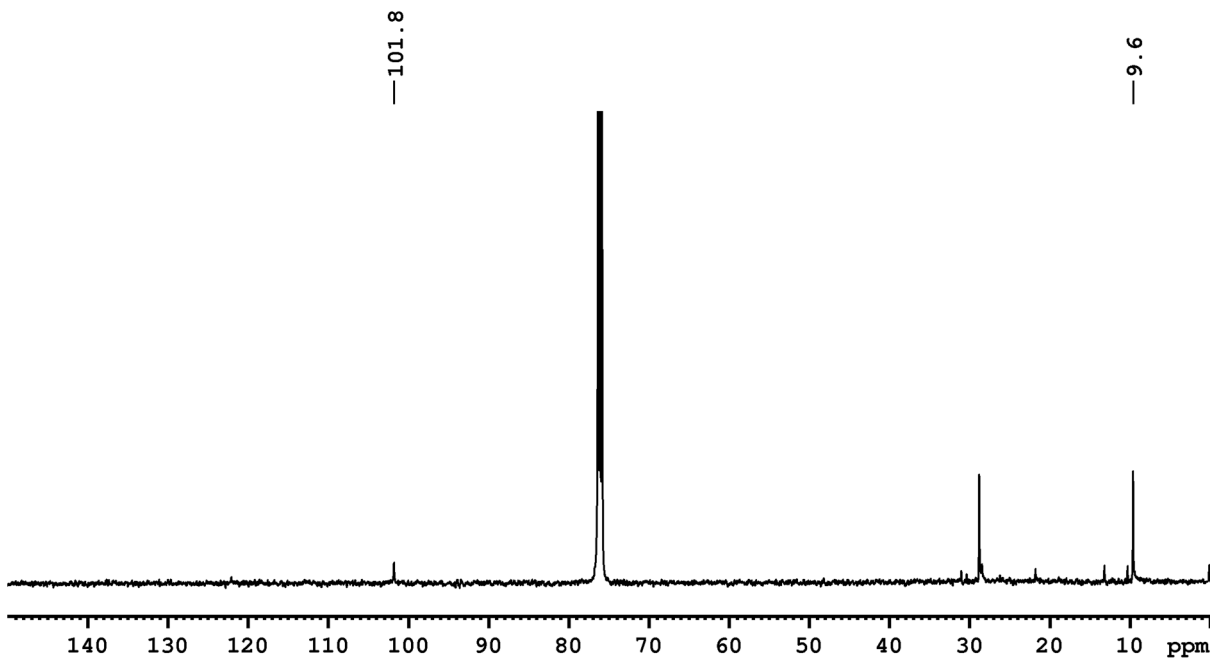


**Figure S9.**  $^{13}\text{C}\{^1\text{H}\}$  NMR spectrum of compound 5.

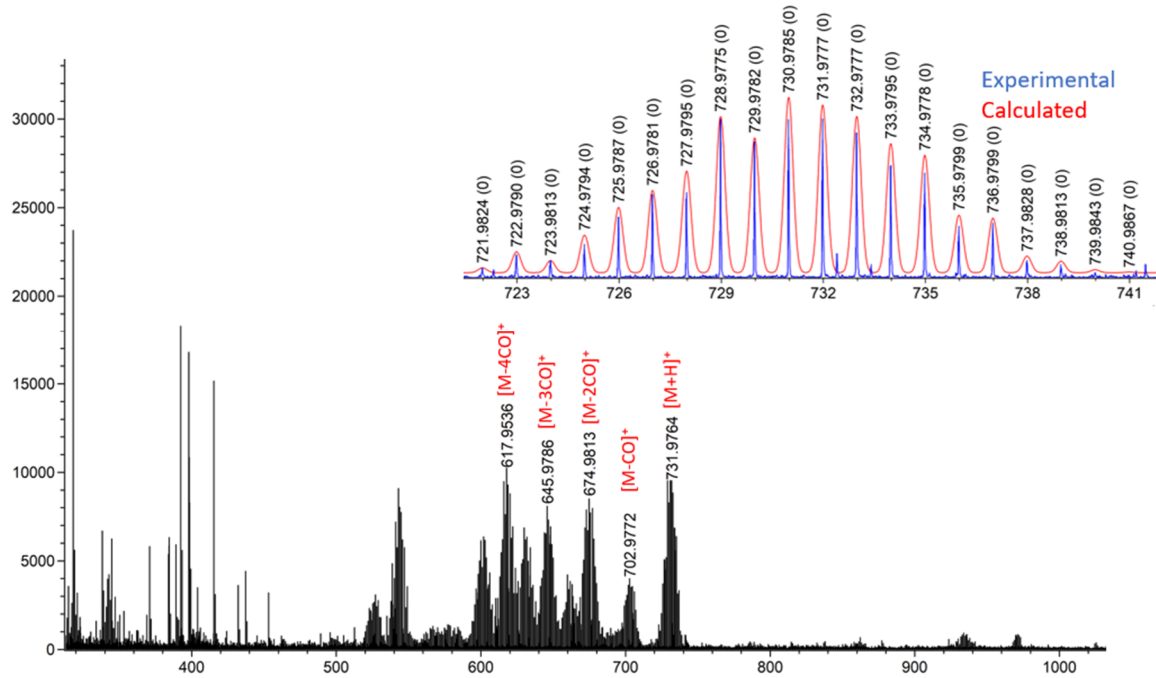


**Figure S10.** ESI-MS spectrum of compound 5 in  $\text{CH}_2\text{Cl}_2$  and MeOH mixture

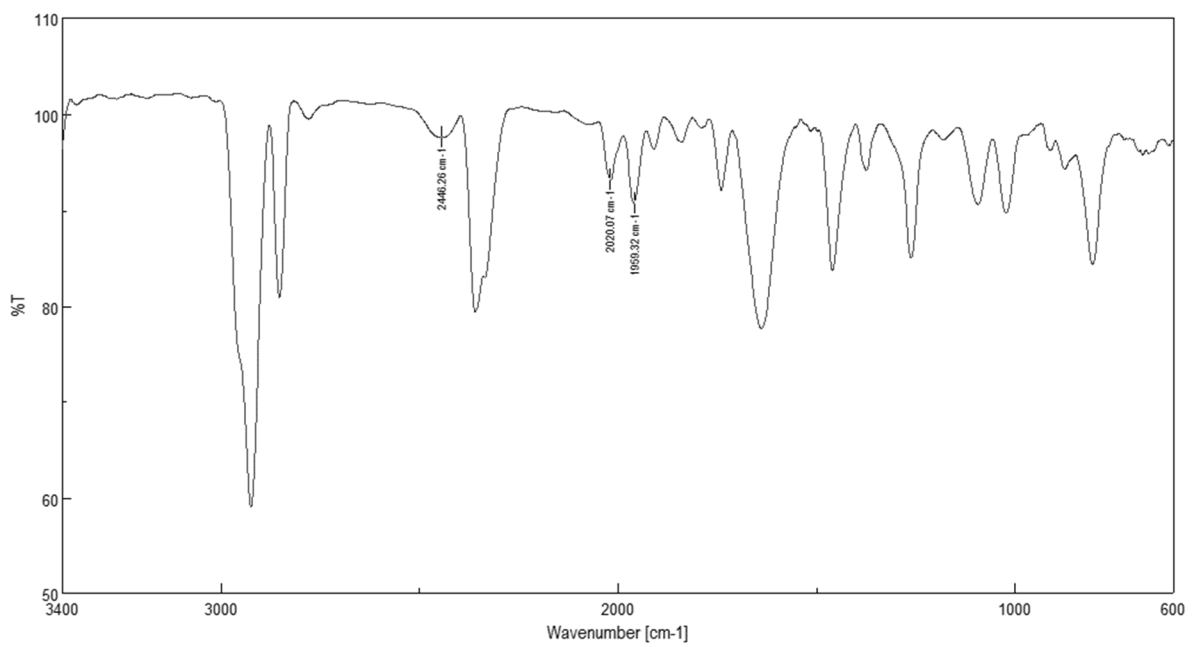


**Figure S11.** IR spectrum of compound 5.

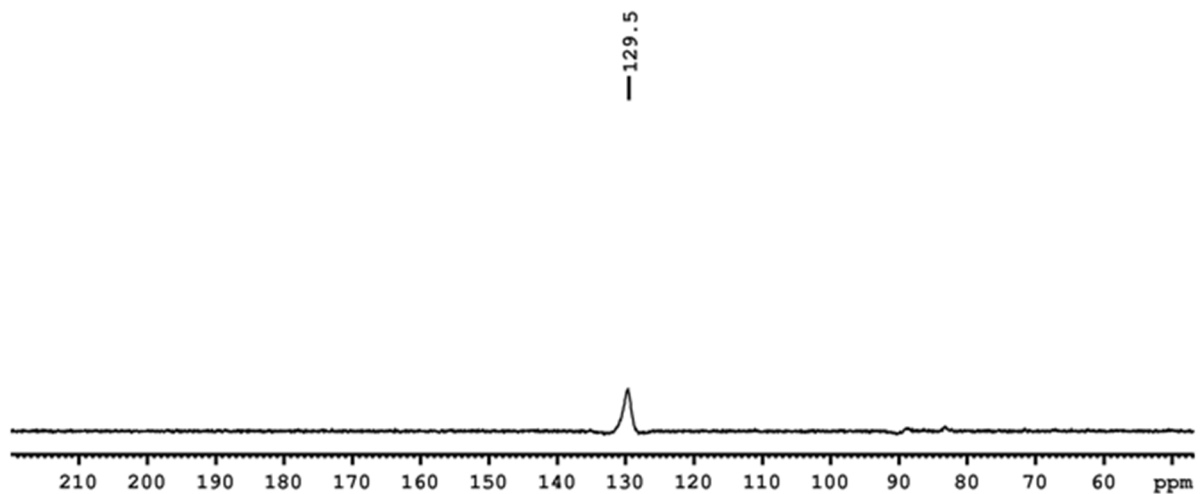


**Figure S12.** <sup>11</sup>B{<sup>1</sup>H} NMR spectrum of compound 6.

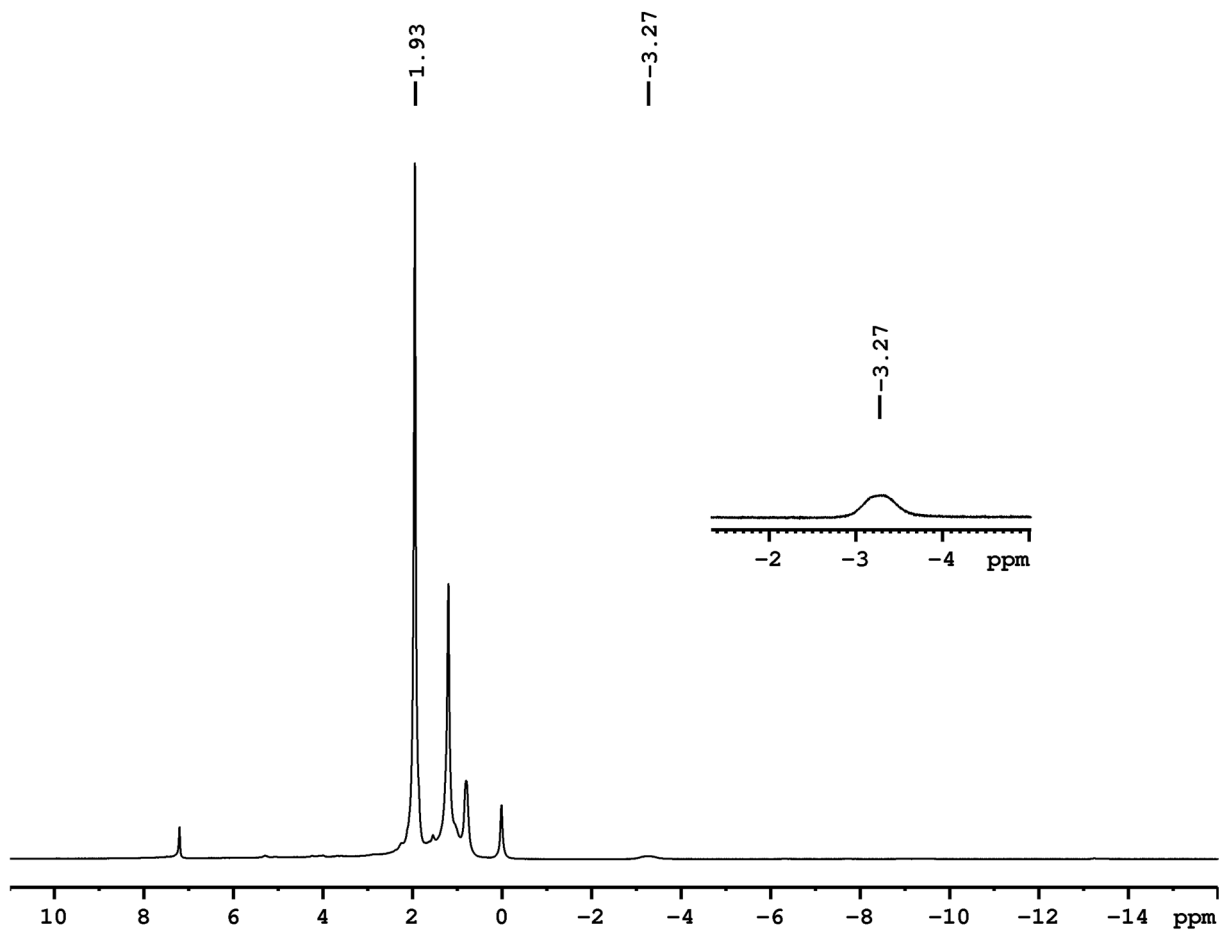


**Figure S13.**  $^1\text{H}$  NMR spectrum of compound 6.

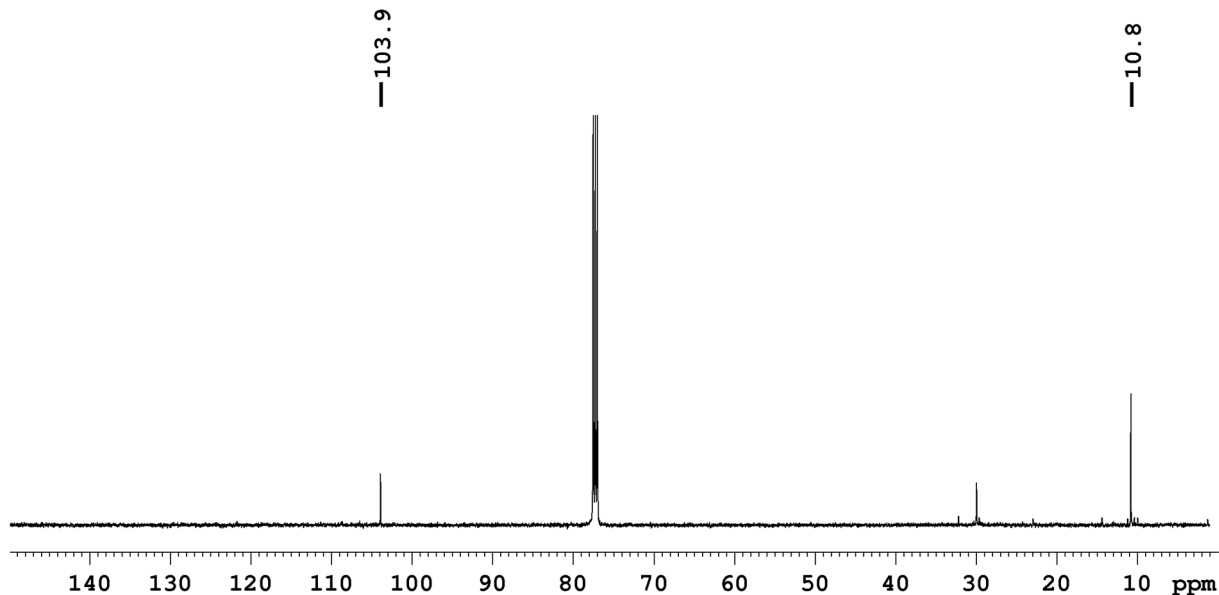


**Figure S14.**  $^{13}\text{C}\{\text{H}\}$  NMR spectrum of compound 6.

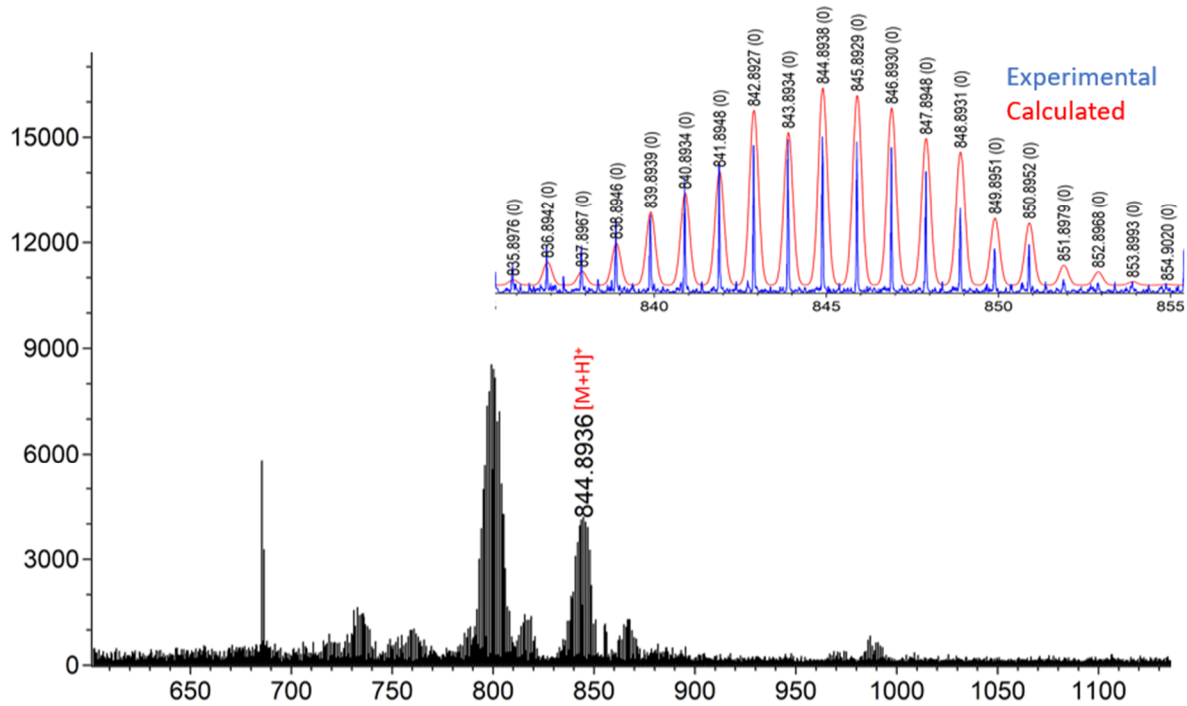


**Figure S15.** ESI-MS spectrum of compound **6** in CH<sub>2</sub>Cl<sub>2</sub> and MeOH mixture.

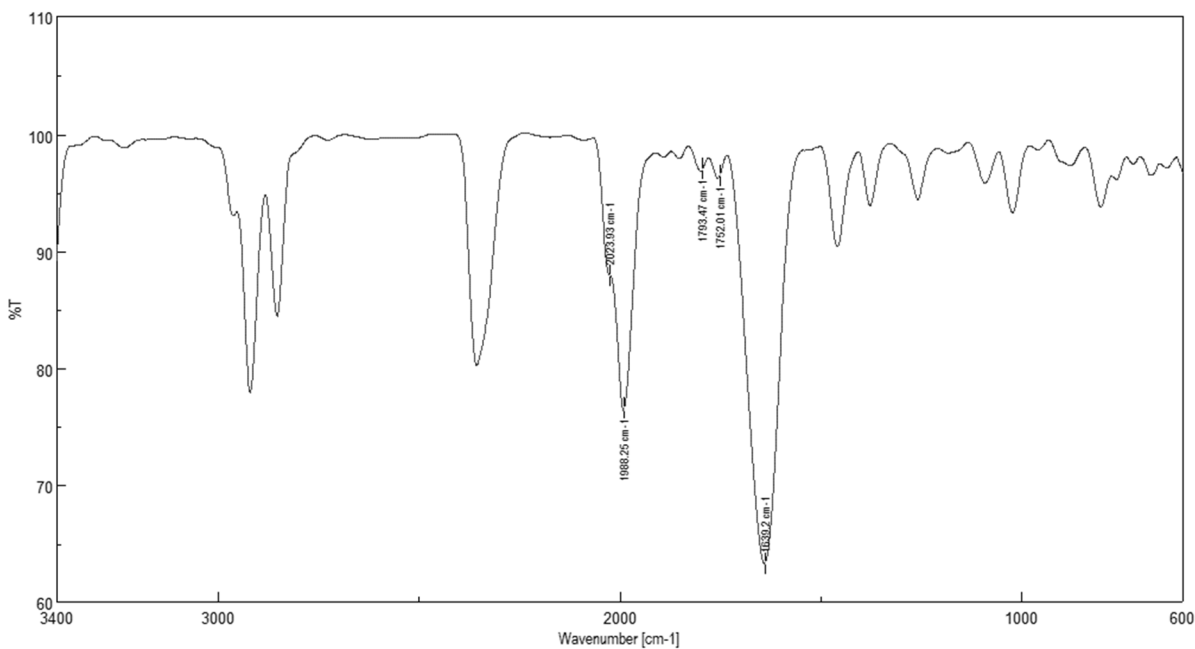


**Figure S16.** IR spectrum of compound **6**.

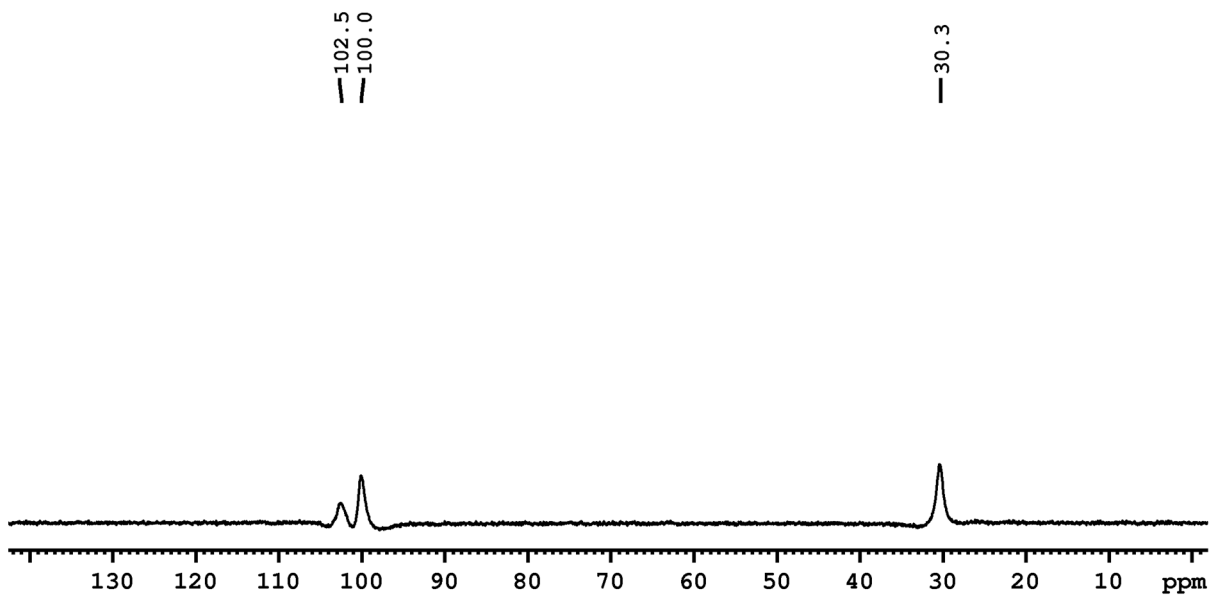


**Figure S17.**  $^{11}\text{B}\{\text{H}\}$  NMR spectrum of compound 8.

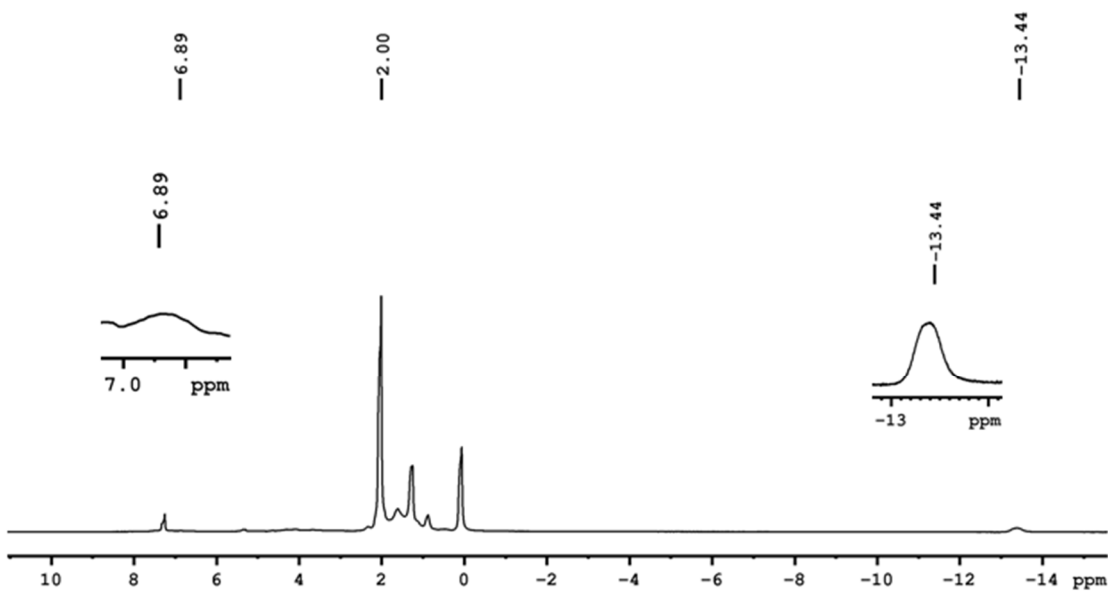


**Figure S18.**  $^1\text{H}$  NMR spectrum of compound 8.

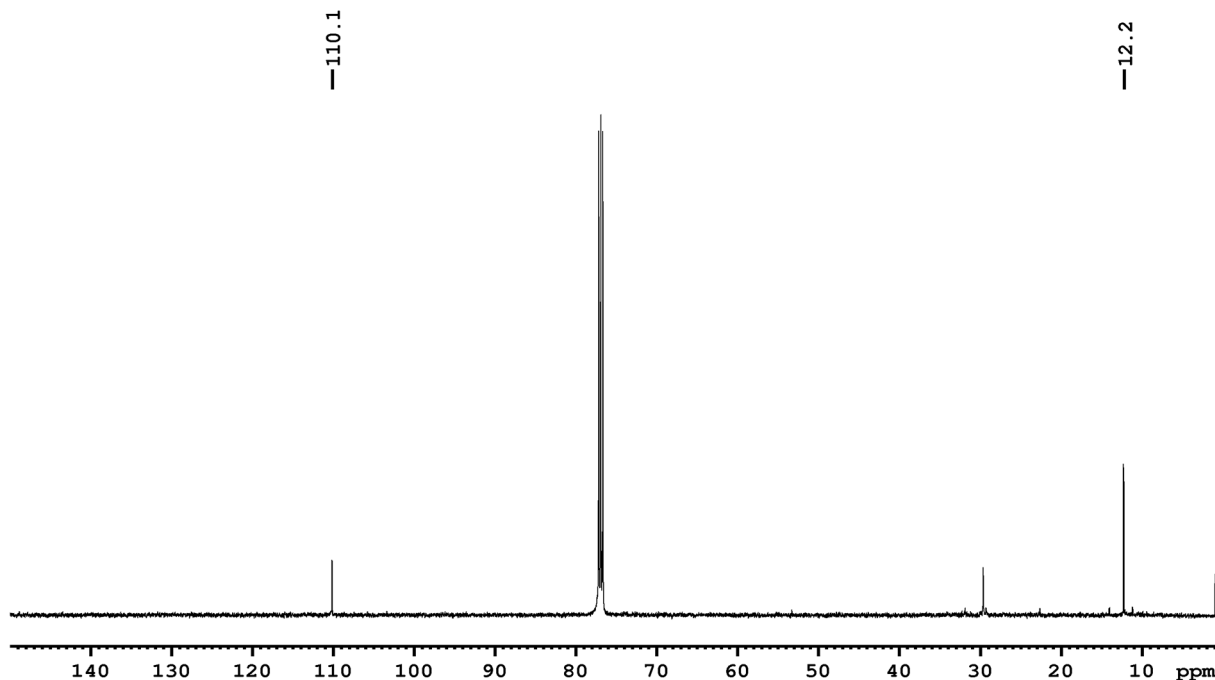


**Figure S19.**  $^{13}\text{C}\{\text{H}\}$  NMR spectrum of compound **8**.

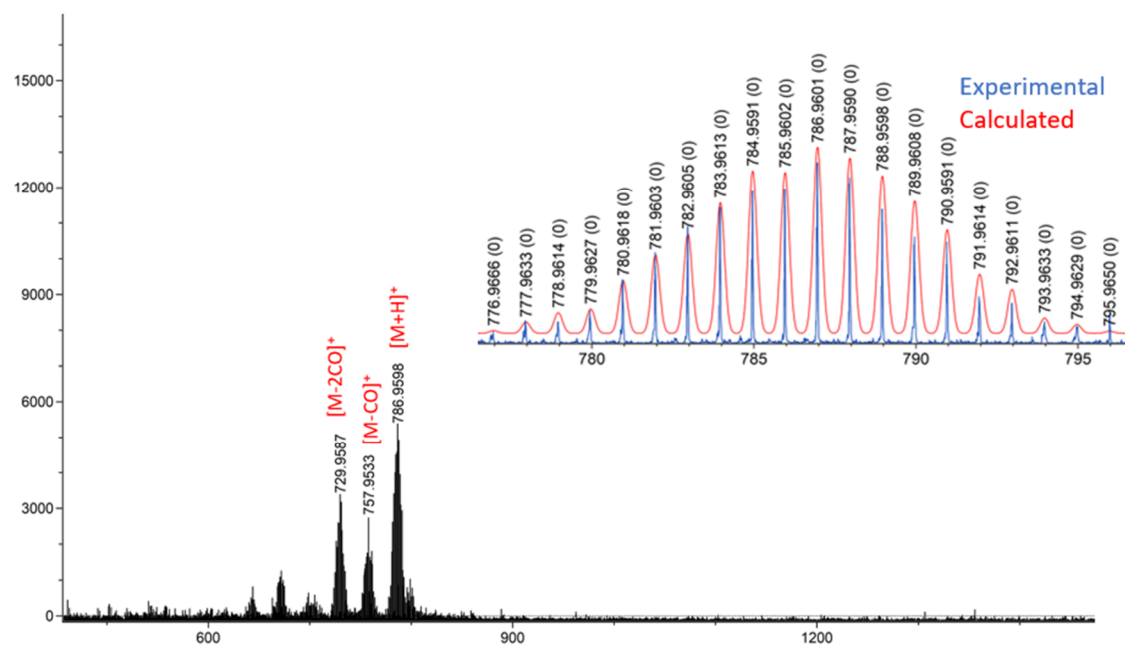


**Figure S20.** ESI-MS spectrum of compound **8** in  $\text{CH}_2\text{Cl}_2$  and MeOH mixture.

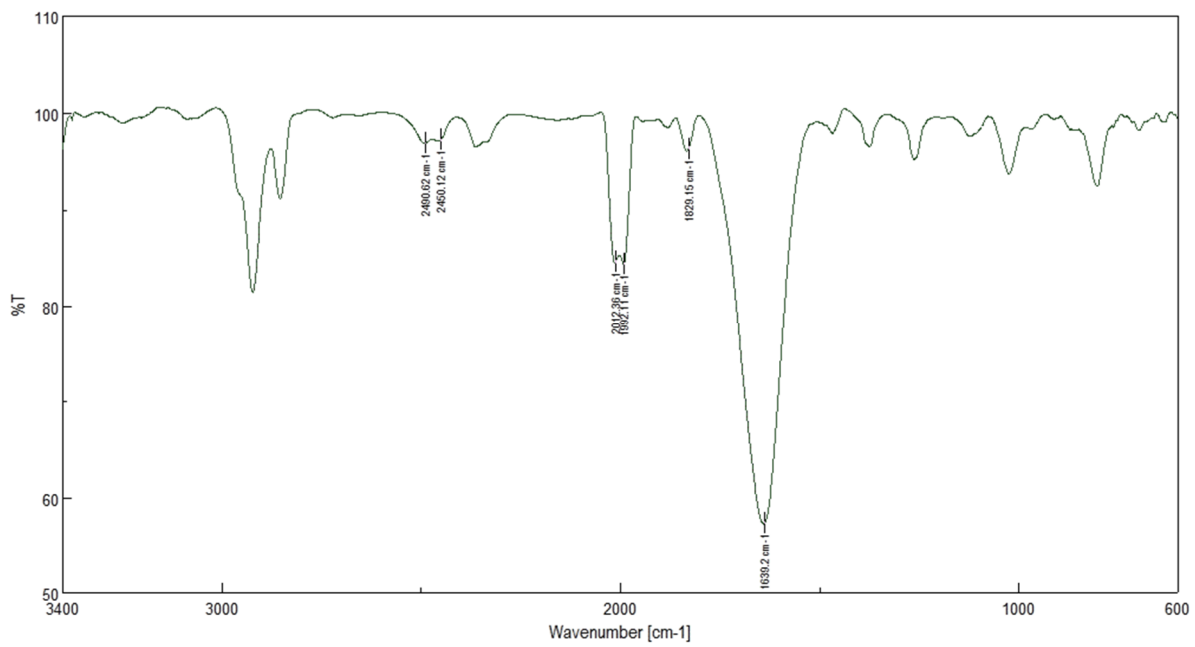


**Figure S21.** IR spectrum of compound **8**.

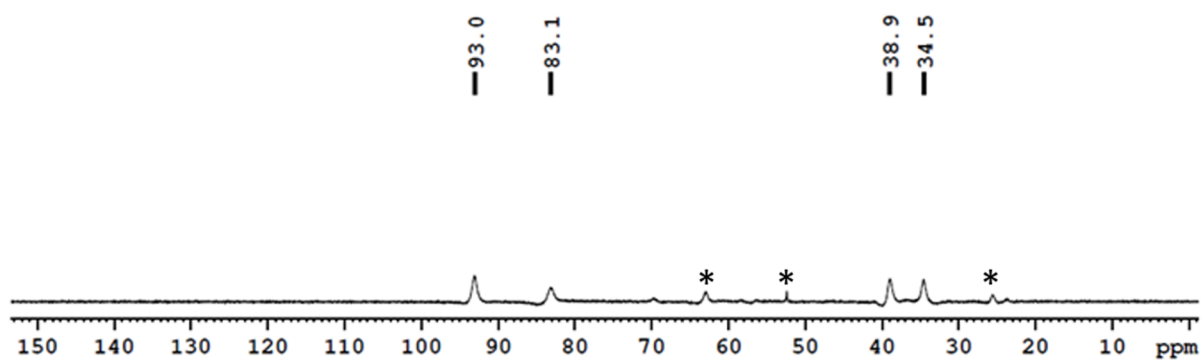


**Figure S22.** <sup>11</sup>B{<sup>1</sup>H} NMR spectrum of compound **9**. (\*peaks corresponding to inseparable impurities)

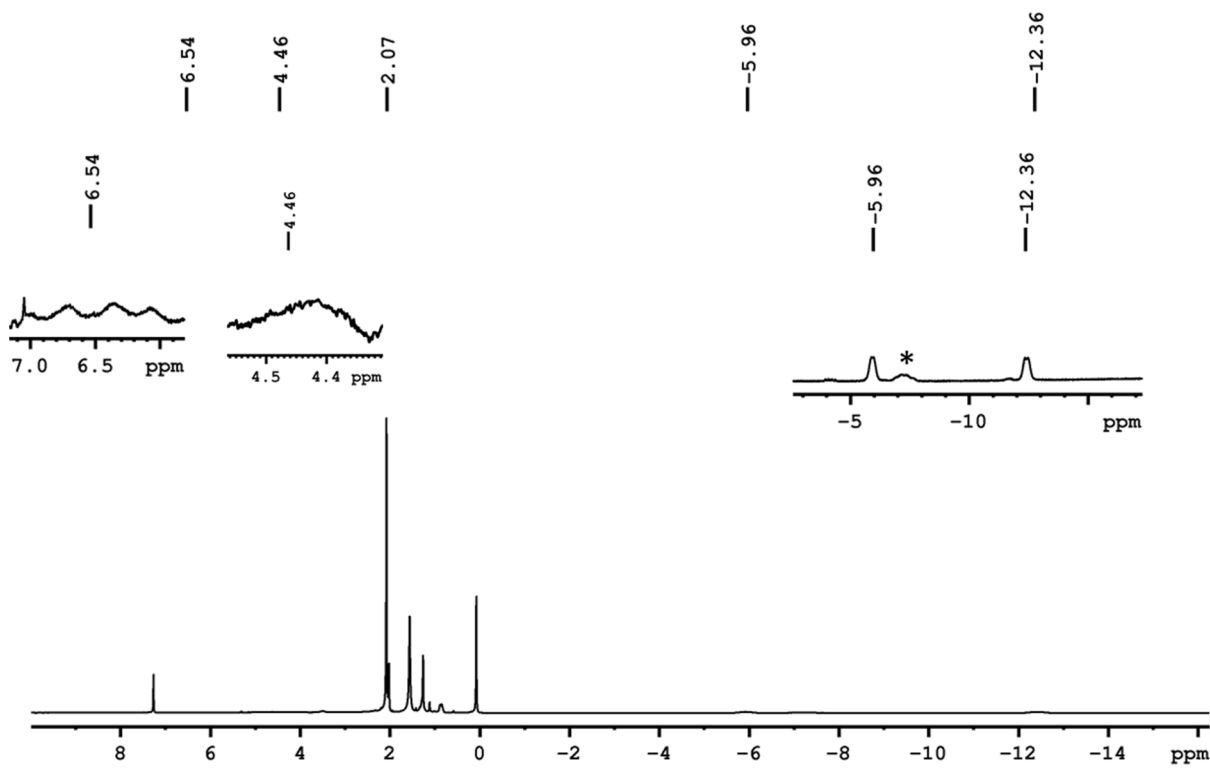


**Figure S23.**  $^1\text{H}$  NMR spectrum of compound **9**. (\*peaks corresponding to inseparable impurities)

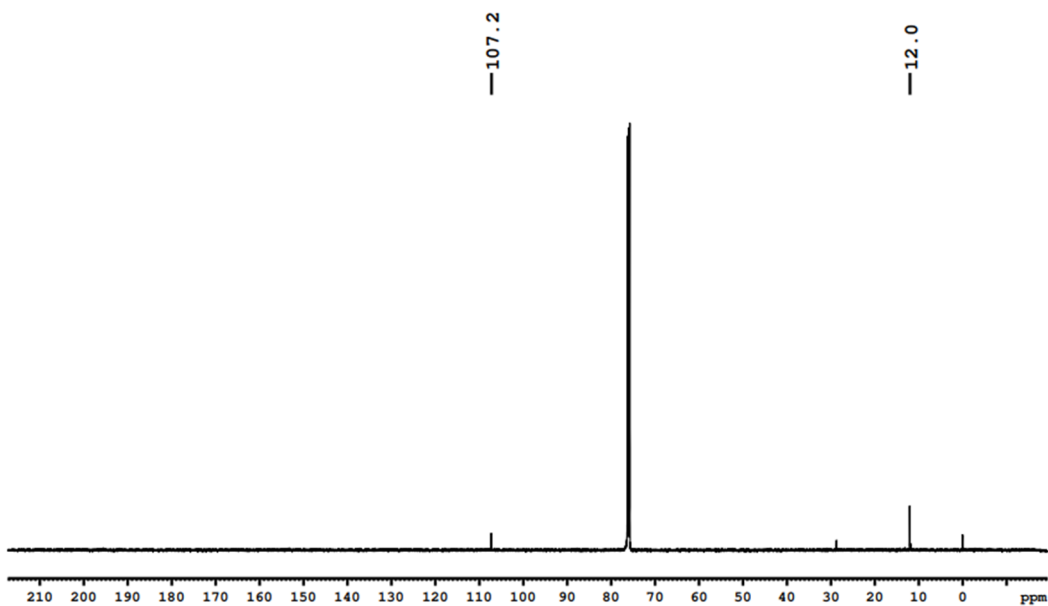


**Figure S24.**  $^{13}\text{C}\{^1\text{H}\}$  NMR spectrum of compound **9**.

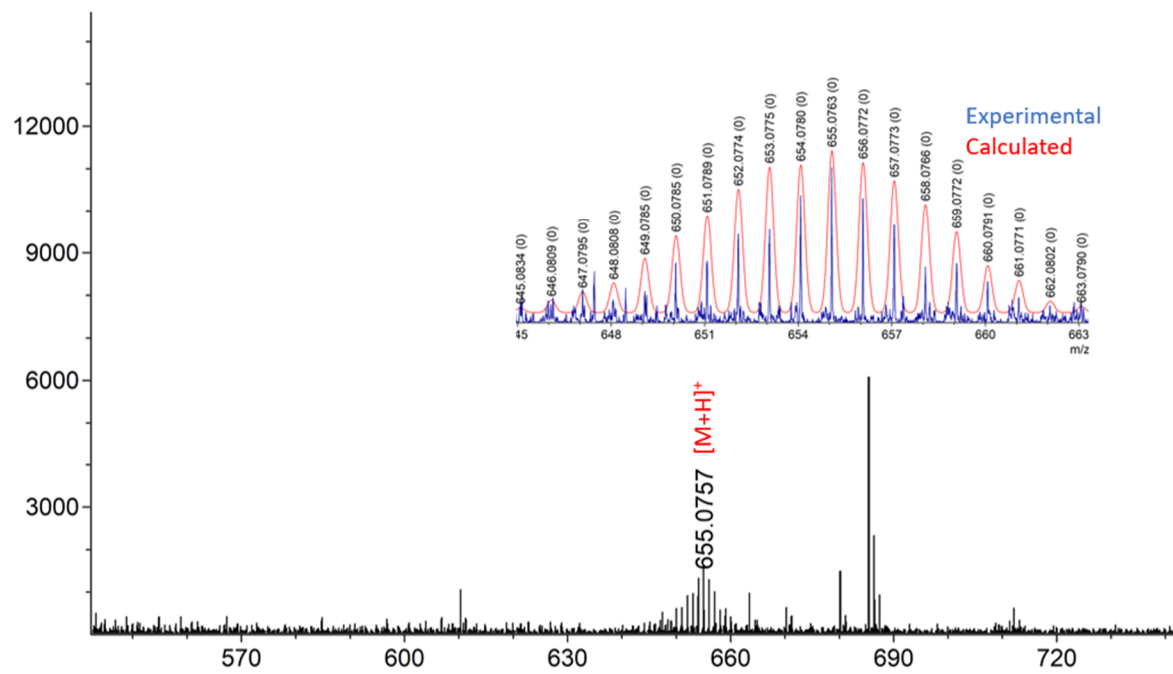


**Figure S25.** . ESI-MS spectrum of compound **9** in  $\text{CH}_2\text{Cl}_2$  and MeOH mixture

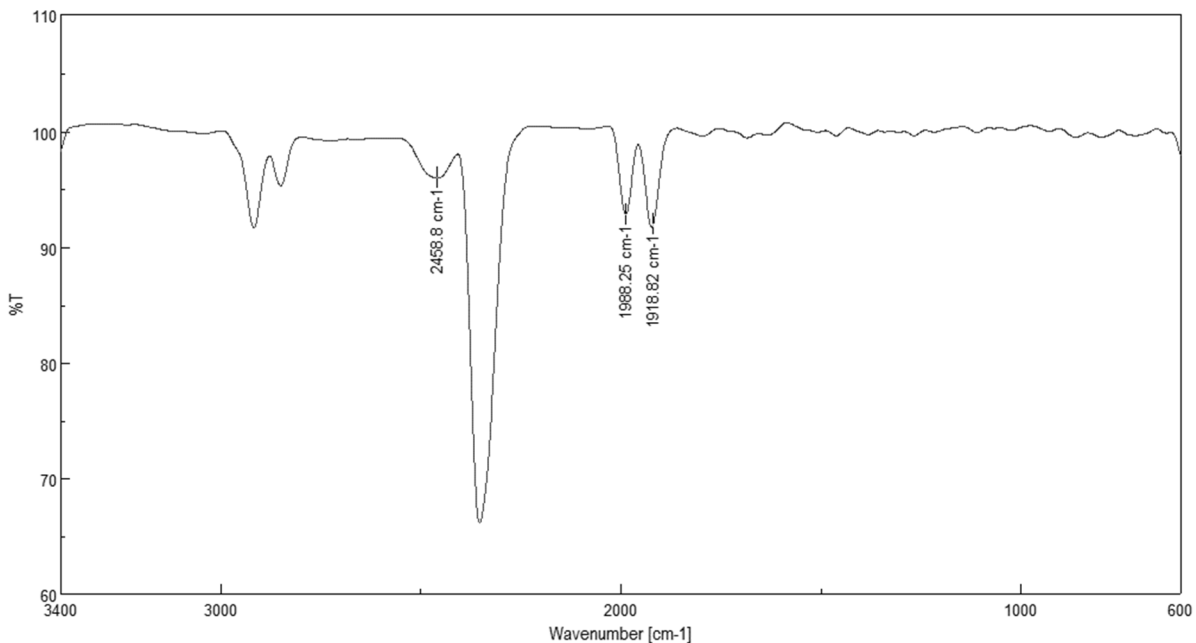


**Figure S26.** IR spectrum of compound **9**.

## II Computational details

All the structures were optimized using the Gaussian 16<sup>[1]</sup> program. The gradient-corrected B3LYP functional<sup>[2]</sup> along with def2-svp basis set<sup>[3]</sup> from EMSL7 Basis Set Exchange Library<sup>[4]</sup> was used for optimization. The model compounds were fully optimized starting from X-ray coordinates in the gaseous state (without solvent). Frequency calculations were carried out for the verification of the nature of the stationary state and to confirm the absence of any imaginary frequency which eventually confirmed the minima on the potential energy hypersurface for all structures. Wiberg bond indices (WBI)<sup>[5]</sup> was generated from natural bond orbital analysis (NBO)<sup>[6]</sup>. All the optimized geometries were drawn by Chemcraft<sup>[7]</sup> visualization program. Laplacian electronic distribution plots and two-dimensional electron density and were generated using the Multiwfn package.<sup>[8]</sup>

**Table S1.** Selected geometrical parameters and Wiberg bond indices (WBI) of **2**, **I**, **II**, **5** and **6**.

<b>2</b>				<b>I</b>			
	Expt.	Cal.	WBI		Expt.	Cal.	WBI
Mo1-Mo2	3.0326(8)	3.096	0.443	Mo1-Mo2	-	3.165	0.308
Mo1-B1	2.354(5)	2.358	0.458	Mo1-B1	-	2.269	0.743
Mo1-B2	2.207(5)	2.283	0.477	Mo1-B2	-	2.147	0.785
Mo1-B3	2.351(6)	2.357	0.460	Mo1-B3	-	2.270	0.743
B1-B2	1.715(8)	1.735	0.624	B1-B2	-	1.805	0.619
B2-B3	1.757(7)	1.737	0.623	B2-B3	-	1.805	0.619
<b>II</b>				<b>5</b>			
	Expt.	Cal.	WBI		Expt.	Cal.	WBI
W1-W2	-	3.194	0.490	Mo1-Mo2	3.058(8)	3.132	0.381
W1-B1	-	2.362	0.436	Mo1-B1	2.25(3)	2.205	0.716
W1-B2	-	2.261	0.565	Mo2-B1	2.23(3)	2.320	0.374
W1-B3	-	2.362	0.436	Co1-B1	2.04(2)	2.133	0.413
B1-B2	-	1.706	0.725	Co1-Mo1	2.796(8)	2.822	0.374
B2-B3	-	1.706	0.725	Co1-Mo2	2.758(8)	2.858	0.353
<b>6</b>							
	Expt.	Cal.	WBI				
Mo1-B1	2.180(5)	2.108	0.859				
Mo2-B1	2.125(5)	2.187	0.621				
Co3-B1	2.022(5)	2.088	0.330				
Co4-B1	2.076(5)	2.057	0.381				
Co4-Mo1	2.7023(8)	2.877	0.306				
Co3-Mo2	2.967(5)	2.741	0.396				

**Table S2.** Comparison between experimental and theoretical chemical shifts of compounds **2**, **I**, **5** and **6**.

<sup>11</sup> B- NMR value (ppm)	2	I	5	6
Experimental	12.9, 3.7	105.5, 34.2	69.7	129.5
Theoretical	-6.8, -8.9, -24.3	104.5, 17.0	47.4	129.4

**Table S3.** Calculated natural charges ( $q_M$ ,  $q_B$  and  $q_E$ ), natural valence population (Pop) and HOMO-LUMO gaps of **2**, **I**, **II**, **5**, and **6**.

Compounds	$q_M$	$q_B$	Pop (M <sub>val</sub> )	Pop (B <sub>val</sub> )	$\Delta E_{H-L}$ (eV)
<b>2</b>	-0.904	-0.146	6.899	3.114	3.370
	-0.787	-0.078	6.779	3.046	
		-0.145		3.113	
<b>I</b>	-0.662	-0.096	6.646	3.059	2.439
	-0.662	-0.262	6.646	2.693	
		-0.096		3.056	
<b>II</b>	-0.353	-0.221	6.342	3.185	2.853
	-0.353	-0.286	6.342	3.248	
		-0.221		3.185	
<b>5</b>	-1.012 (Mo)	-0.136	7.017 (Mo)	2.818	2.901
	-0.931 (Mo)		6.948 (Mo)		
	-1.489 (Co)		10.476 (Co)		
<b>6</b>	-1.186 (Mo)	-0.497	7.199 (Mo)	2.441	2.585
	-0.961 (Mo)		6.957 (Mo)		
	-0.937 (Co)		9.925 (Co)		
	-1.346 (Co)		10.330 (Co)		

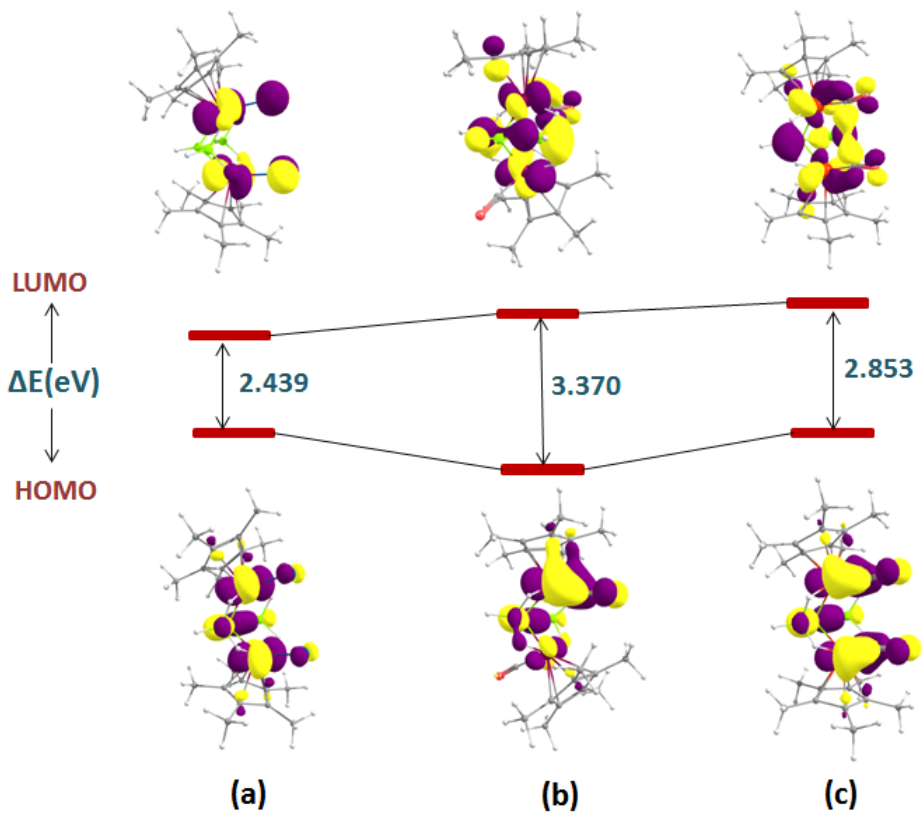


**Figure S27.** Comparison of HOMO-LUMO gap in **2(a)**, **I(b)**, **II(c)**.

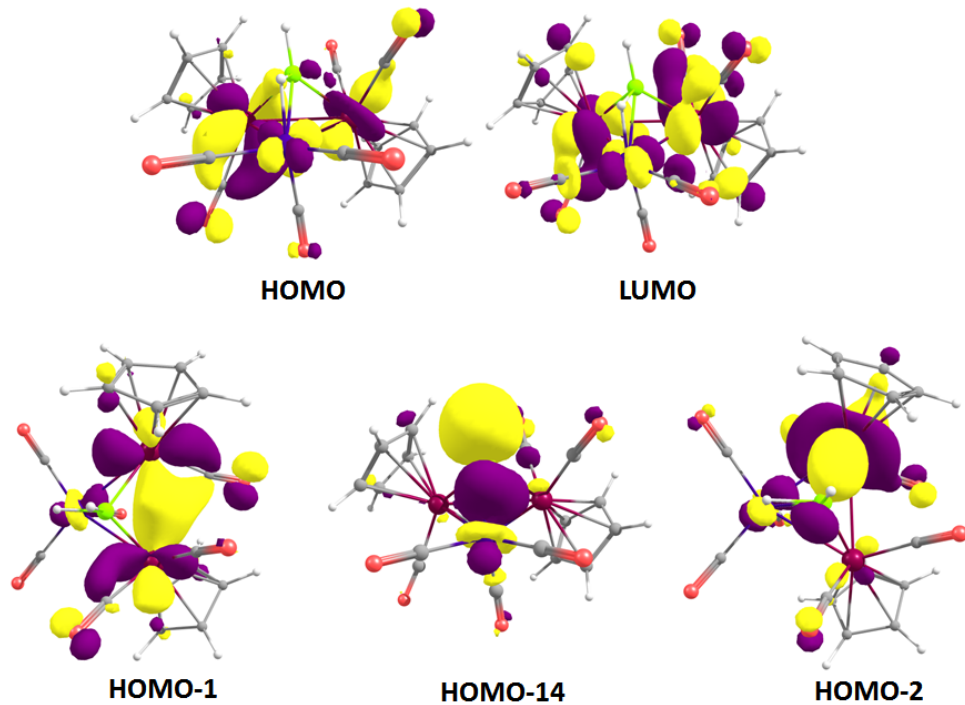


**Figure S28.** Selected frontier molecular orbitals of **5**.

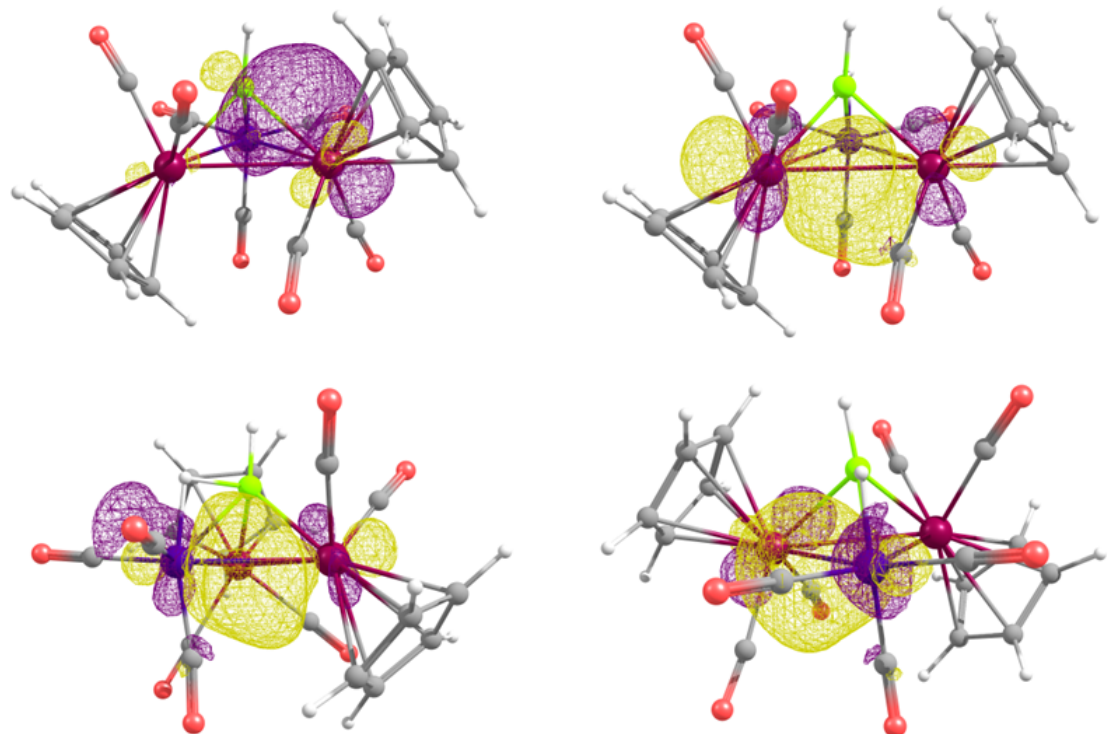


**Figure S29.** Selected natural bonding orbitals of **5**.

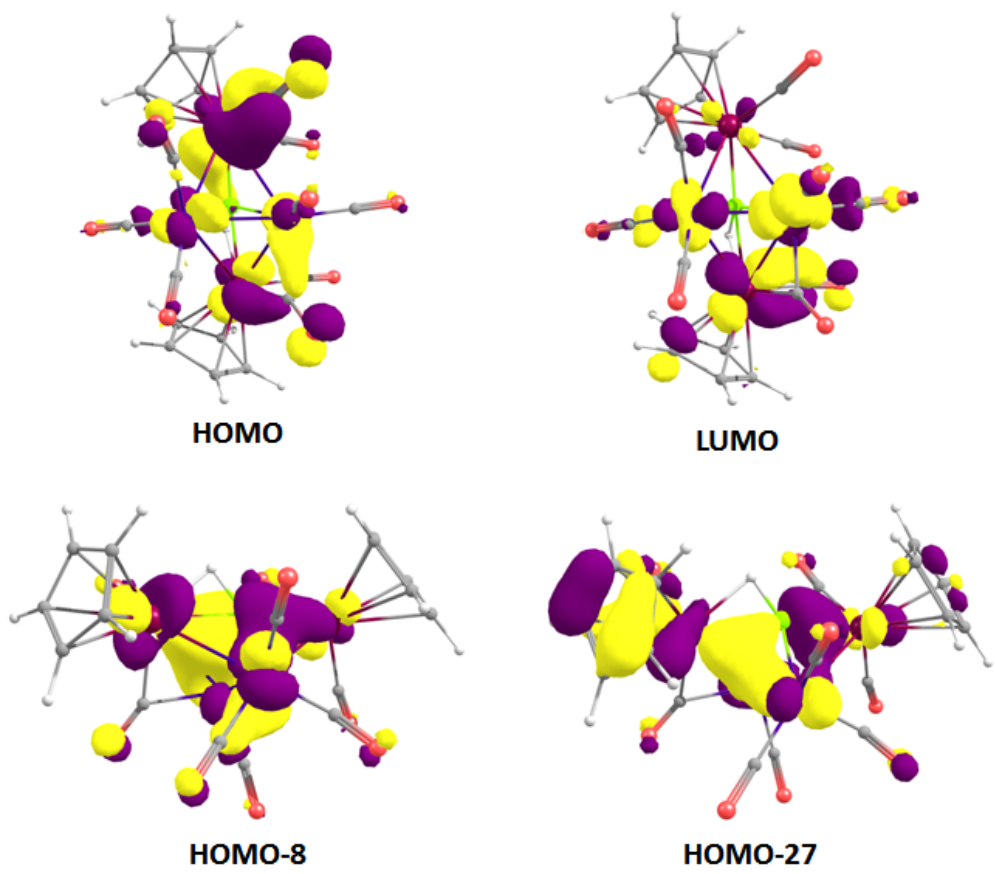


**Figure S30.** Selected frontier molecular orbitals of **6**.

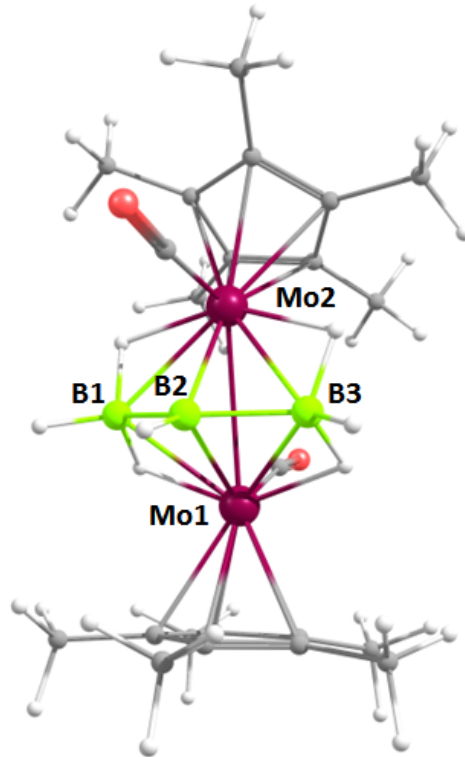


**Figure S31.** Optimized geometry of **2**.

Total Energy = -1222.68045653 a. u.

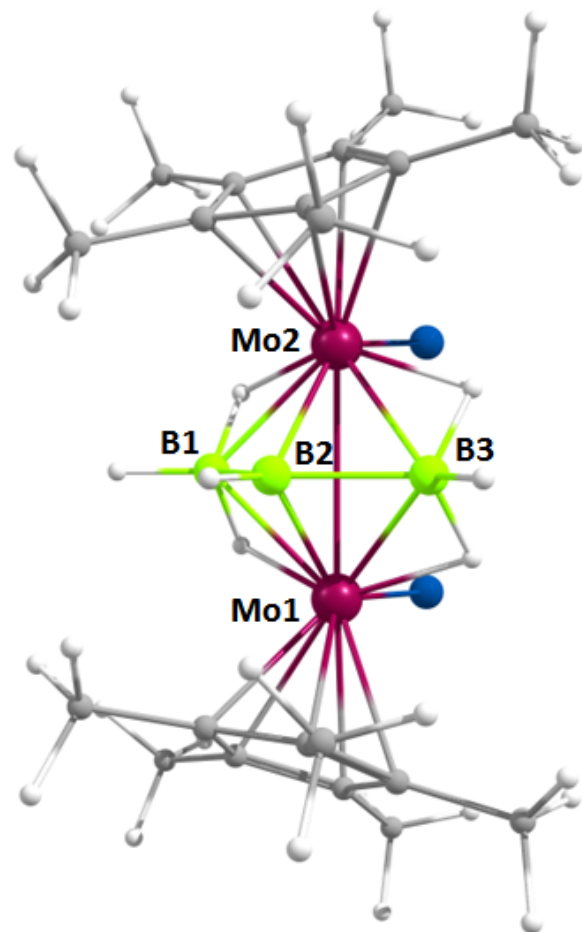


**Figure S32.** Optimized geometry of **I**.

Total Energy = -1916.41218190 a. u.

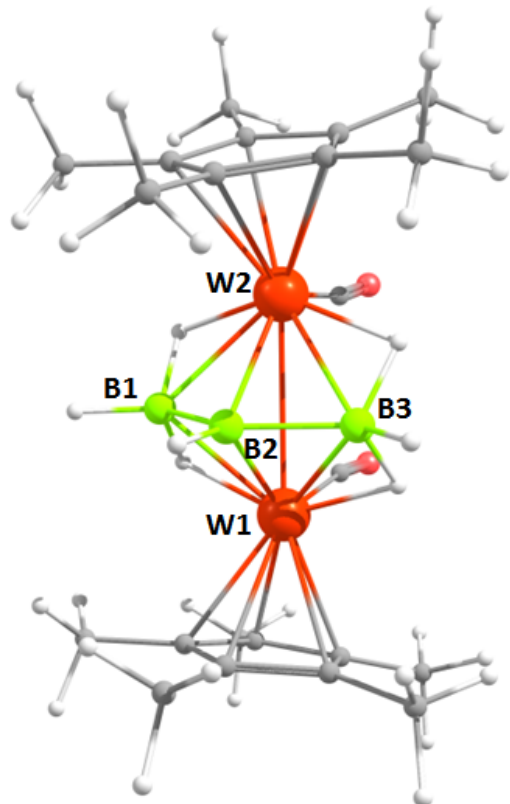


**Figure S33.** Optimized geometry of **II**.

Total Energy = -1220.43597081 a. u.

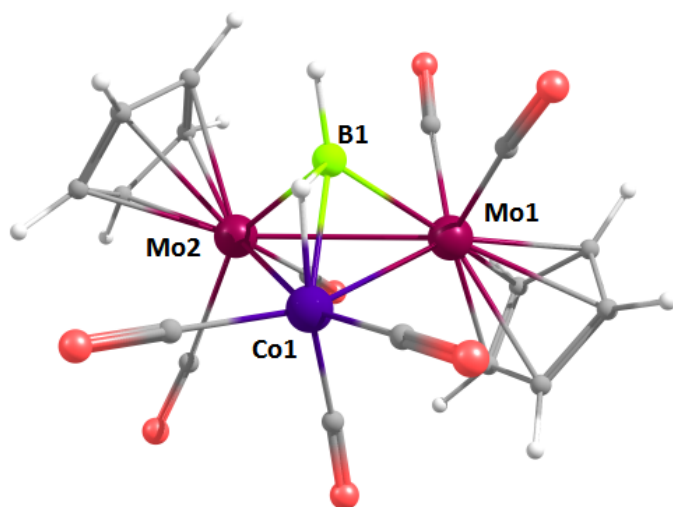


**Figure S34.** Optimized geometry of **5**.

Total Energy = -2726.43589030 a. u.

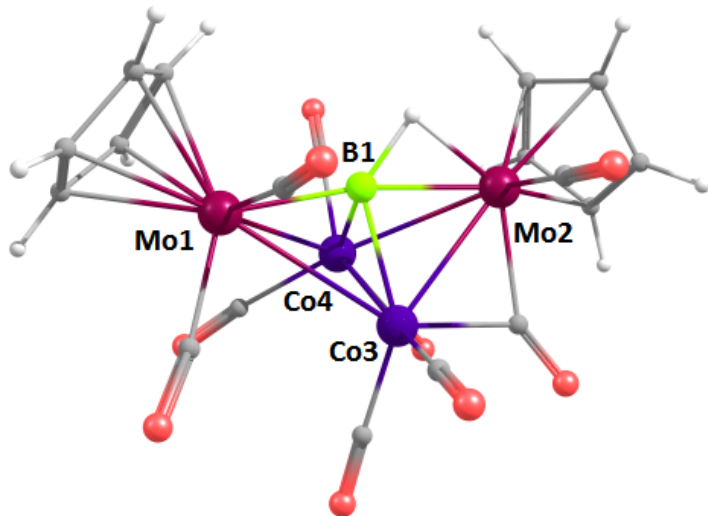


**Figure S35.** Optimized geometry of **6**.

Total Energy = -4335.47672384 a. u.

---

### References:

- 1 Frisch, M. J.; Trucks, G. W.; Schlegel, H. B.; Scuseria, G. E.; Robb, M. A.; Cheeseman, J. R.; Scalmani, G.; Barone, V.; Mennucci, B.; Petersson, G. A.; Nakatsuji, H.; Caricato, M.; Li, X.; Hratchian, H. P.; Izmaylov, A. F.; Bloino, J.; Zheng, G.; Sonnenberg, J. L.; Hada, M.; Ehara, M.; Toyota, K.; Fukuda, R.; Hasegawa, J.; Ishida, M.; Nakajima, T.; Honda, Y.; Kitao, O.; Nakai, H.; Vreven, T.; Montgomery, J. A., Jr.; Peralta, J. E.; Ogliaro, F.; Bearpark, M.; Heyd, J. J.; Brothers, E.; Kudin, K. N.; Staroverov, V. N.; Keith, T.; Kobayashi, R.; Normand, J.; Raghavachari, K.; Rendell, A.; Burant, J. C.; Iyengar, S. S.; Tomasi, J.; Cossi, M.; Rega, N.; Millam, J. M.; Klene, M.; Knox, J. E.; Cross, J. B.; Bakken, V.; Adamo, C.; Jaramillo, J.; Gomperts, R.; Stratmann, R. E.; Yazyev, O.; Austin, A. J.; Cammi, R.; Pomelli, C.; Ochterski, J. W.; Martin, R. L.; Morokuma, K.; Zakrzewski, V. G.; Voth, G. A.; Salvador, P.; Dannenberg, J. J.; Dapprich, S.; Daniels, A. D.; Farkas, O.; Foresman, J. B.; Ortiz, J. V.; Cioslowski, J.; Fox, D. J. Gaussian 09, revision C.01; Gaussian, Inc.: Wallingford, CT, **2010**.
- 2 Lee, C.; Yang, W.; Parr, R. G. Development of the Colle-Salvetti Correlation-Energy Formula into a Functional of the Electron Density. *Phys. Rev. B*. **1988**, *37*, 785–789.
- 3 Perdew, J. P.; Burke, K.; Ernzerhof, M. Generalized Gradient Approximation Made Simple. *Phys. Rev. Lett.* **1996**, *77*, 3865–3868.
- 4 Pritchard, B. P.; Altarawy, D.; Didier, B.; Gibson, T. D.; Windus, T. L. New Basis Set Exchange: An Open, Up-to-Date Resource for the Molecular Sciences Community. *J. Chem. Inf. Model.* **2019**, *59*, 4814–4820.

- 5 Wiberg, K. Application of the pople-santry-segal CNDO method to the cyclopropylcarbinyl and cyclobutyl cation and to bicyclobutane. *Tetrahedron* **1968**, *24*, 1083–1096.
- 6 Glendening, E. D.; Badenhoop, J. K.; Reed, A. E.; Carpenter, J. E.; Bohmann, J. A.; Morales, C. M.; Landis, C. R.; Weinhold, F. *NBO Program 6.0; Theoretical Chemistry Institute, University of Wisconsin: Madison, WI, USA*, **2013**.
- 7 Zhurko, G. A. <http://www.chemcraftprog.com>
- 8 Lu, T.; Chen, F. Multiwfn: a multifunctional wavefunction analyzer. *J. Comput. Chem.* **2012**, *33*, 580–592.